Preprints of the 21st IFAC World Congress (Virtual)
Berlin, Germany, July 12-17, 2020

In-Line Estimation of the Magnetization Curve of Steel Strips in a Continuous Induction Furnace ⋆

L. Jadachowski * **F. Roetzer** ** **A. Steinboeck** ** **A. Kugi** *,**

* *Christian Doppler Laboratory for Model-Based Process Control in the Steel Industry, Automation and Control Institute, TU Wien, Gußhausstraße 27-29, 1040 Vienna, Austria (e-mail: {jadachowski,kugi}@acin.tuwien.ac.at)*
** *Automation and Control Institute, TU Wien, Gußhausstraße 27-29, 1040 Vienna, Austria (e-mail: {roetzer,steinboeck}@acin.tuwien.ac.at)*

Abstract: An in-line parameter estimation strategy for continuous inductive heating of ferromagnetic steel strips is developed and investigated. During strip processing in a longitudinal flux induction furnace, the parameters of the magnetization curve (B-H curve) of the strip material are identified by a moving horizon estimator (MHE). The estimator uses a tailored 2D spatial-temporal model of the furnace which takes into account both the thermal and the electromagnetic subsystem. Other model parameters are identified in a scenario, where the magnetization curve of the strip is known. For model validation, the simulated strip temperature at the furnace exit is compared with measurements. To approximate the solution of the nonlinear Maxwell equations, the effective magnetization approach is applied. Here, a sophisticated hysteretic magnetization model is avoided in favor of the computing time, while magnetic saturation effects in the strip are still captured. The developed MHE is validated in a simulation scenario based on a strip with a known magnetization curve.

Keywords: Moving horizon estimator, Parameter estimation, B-H curve, Effective magnetization, Longitudinal flux induction, Nonlinear Maxwell equations, Parabolic PDE.

1. INTRODUCTION

Inductive (re-)heating (IH) systems for thin steel strips have been developed for more than seven decades (Rudnev et al., 2017). Already in the early 1940s, first investigations and analytical calculations of longitudinal flux induction heaters (LFIHs) for continuously moving strips were reported by Baker (1945). In a conventional LFIH, a solenoid coil surrounds the axially moving strip and the resulting magnetic flux direction equals the direction of the strip movement. Provided that the strip material is electrically conductive, induced eddy currents complete their paths within the cross-sections of the strip and generate heat in the strip (Joule heating effect).

Heat treatment is the basic function of IH systems. An extra benefit of IH can be the continuous identification or monitoring of material properties of the strip. In particular, if the strip temperature is measured both at the entrance and at the exit of an LFIH, magnetic properties of the strip in terms of a relation between the magnetic flux density $\mathcal{B}$ and the induced magnetic field strength $\mathcal{H}$ can be estimated. This relation depends on to chemical composition, fabrication, and temperature of the ferromagnetic strip (Bozorth, 2003). However, its accurate estimate is very desirable in hot-dip galvanizing lines. Saxinger et al. (2018) reported that knowledge of magnetic properties at elevated temperatures has to be taken into account when calculating electromagnetic forces for active vibration and position control in such production lines. Knowledge of the magnetic behavior is also crucial when applying micromagnetic methods for the estimation of phase transformations and mechanical properties in steel production. To control the phase volume ratio of multi-phase steels, an electromagnetic sensor (EMspec) developed by Shen et al. (2019) requires relative permeability values of single phases and partially transformed microstructures. These values are calculated from a microstructure-permeability model presented by Hao et al. (2010). The model uses a linear magnetic material law with the single phase low field permeability and electric resistivity values as inputs. The so-called EMG IMPOC system uses measurements of the gradient of the residual magnetic field strength to estimate the tensile strength and the yield point of ferromagnetic strips. The system needs the magnetic properties of the strip as input parameters of the underlying electromagnetic solver and for the calculation of the sensor output (Skarlatos et al., 2016).

A thorough review of the relevant literature reveals an absence of solutions where high-power IH furnaces are used beyond heat treatment as soft sensors for magnetic material properties at high temperatures. Hence, in this paper, an in-line estimation strategy for a nonlinear magnetic constitutive equation during strip processing at elevated temperatures in an LFIH is developed. In particular, the

⋆ The financial support by the Christian Doppler Research Association, the Austrian Federal Ministry for Digital and Economic Affairs, and the National Foundation for Research, Technology and Development, and voestalpine Stahl GmbH is gratefully acknowledged.

goal is to estimate the scalar magnetization relation of the heated strip material, most commonly expressed in terms of a $B(H)$ curve, where B and H denote norm amplitudes of the magnetic flux density $\mathcal{B}(\mathbf{x}, t)$ and the field strength $\mathcal{H}(\mathbf{x}, t)$, respectively. As a basis for this estimation, a finite-element (FE) model of the LFIH is proposed. The model takes into account time-harmonic Maxwell's equations describing electromagnetic phenomena in the heating zone of the LFIH and the heat conduction equation in the strip in terms of partial differential equations (PDEs). However, in the model, the nonlinear magnetic behavior is approximated by means of effective quantities B_{eff} and H_{eff} of a fictitious linear material and implemented in terms of the $H_{\text{eff}}(B_{\text{eff}})$ function. The determination of the B_{eff}-H_{eff} relation is based on the conservation of magnetic energy stored in the strip. This approximation simplifies the solution of the nonlinear Maxwell's equations to the solution of a set of linear equations. The proposed FE model serves as a basis for the design of a real-time moving horizon estimator (MHE) for the parameters of a nonlinear material law, i.e. the B-H curve. The estimator uses measurements of the heating power of the LFIH, the strip velocity, the strip temperatures at the inlet and the outlet of the LFIH as well as the ambient temperature in the furnace. The estimation performance is validated in a simulation scenario based on strips where the B-H curve is known from experimental offline measurements.

The paper is structured as follows: In Section 2, the development of a 2-dimensional FE model consisting of a thermal and an electromagnetic subsystem is developed. In Section 3, the derived model is parametrized and validated using measurements. The MHE scheme is introduced in Section 4. Estimation results obtained with the validated model are presented and analyzed in Section 5. Final remarks given in Section 6 conclude the paper.

Notation: Arguments of functions are omitted whenever they are clear from the context. $\Delta T(\mathbf{x}, t)$ denotes the Laplacian and $\nabla T(\mathbf{x}, t)$ is the temperature gradient with respect to the spatial coordinates $\mathbf{x} = (x, y)$. ∂_* denotes the partial derivative with respect to $*$. Moreover, $\nabla\times$ and $\nabla\cdot$ represent the curl and the divergence operators.

2. MATHEMATICAL MODEL

The LFIH under consideration is used by voestalpine Stahl GmbH for heat treatment of steel strips in a hot-dip galvanizing line located in Linz, Austria. The simplified geometry of the IH system is presented in Fig. 1. It shows a quarter view of the LFIH. The system consists of two water-cooled rectangular solenoid coils (length L_c, width W_c), a screening jacket, and the steel strip (length L_s, width W_s, thickness B_s), which is axially moving with the velocity $v(t)$. The strip enters the LFIH at $x = 0$ with a mean temperature $\theta_0(t)$ and leaves it at $x = L_s$ with the temperature $\theta_L(t)$ (cf. Fig. 2). At these positions, the mean strip surface temperature can be measured. When supplying alternating current (AC) to the coils, the strip undergoes inductive heating.

For reasons of computational efficiency, a 2-dimensional (2D) distributed-parameter model of the LFIH is formulated. The 2D geometry of the longitudinal cross-section of the LFIH is shown in Fig. 2. It comprises the spatial

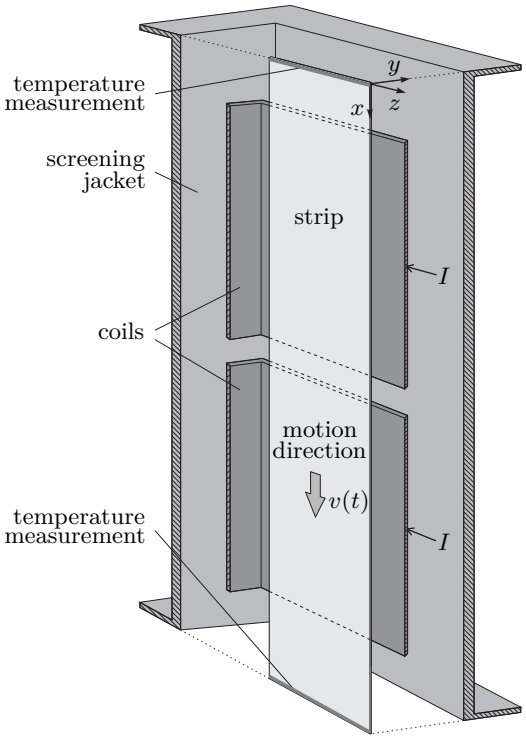

Fig. 1. A simplified quarter view of the LFIH.

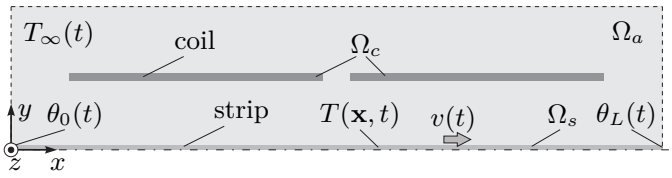

Fig. 2. 2D geometry of the LFIH (not to scale).

domain Ω_s of the strip, Ω_c of the coils and Ω_a of the surrounding air volume. The computational domain $\Omega = \Omega_s \cup \Omega_c \cup \Omega_a$ covers the volume inside the screening jacket. The 2D approximation is justified by the assumption of a homogeneous magnetic field $\mathcal{H}$ and strip temperature T along the direction z. It is known that LFIHs are normally not sensitive to an off-center strip position within the induction coil (see, e.g., Rudnev et al., 2017). Hence, a potential off-center strip position is neglected in the mathematical model presented in the following subsections.

2.1 Heat Conduction PDE

The temperature evolution in the strip depends on the time t and the spatial coordinates $\mathbf{x} = (x, y) \in \Omega_s$. It is modeled by the 2D parabolic PDE

$$\rho c_p \big(\partial_t T(\mathbf{x}, t) + v(t)\partial_x T(\mathbf{x}, t)\big) = \lambda \Delta T(\mathbf{x}, t) + \dot{q}_{\text{IH}}(\mathbf{x}, I) \quad (1)$$

with the 2D temperature profile $T(\mathbf{x}, t)$, the mass density ρ, the specific heat capacity c_p, and the thermal conductivity λ. In view of moderate changes of the strip temperature in the LFIH, c_p and λ are assumed to be constant. The source term $\dot{q}_{\text{IH}}(\mathbf{x}, I)$ on the right hand side of (1) describes the volumetric heat generation due to IH. It depends on $\mathbf{x}$ and the system input $I(t)$. The system input of the model is the RMS value of the sinusoidal AC current with angular frequency ω. It is assumed that $I(t)$ can be measured and is controlled by a subordinate current

control loop. Its maximum value $I_{\max}$ is restricted by the maximum net heating power of the LFIH. In case that $I(t)$ cannot be measured, the heat source due to IH can be estimated from the energy balance and by using only the secondary current of the equivalent circuit diagram of the underlying electromagnetic field problem, (see, e.g., Roetzer et al., 2020).

The PDE (1) is supplemented by Dirichlet boundary conditions (BCs) for $\Gamma_D := \{\mathbf{x} \in \mathbb{R}^2 \mid x = 0,\ 0 \leq y \leq B_s/2\}$ and Neumann BCs for $\Gamma'_N := \{\mathbf{x} \in \mathbb{R}^2 \mid y = B_s/2,\ 0 \leq x \leq L_s\}$ and $\Gamma''_N := \partial\Omega_s \setminus (\Gamma_D \cup \Gamma'_N)$ as

$$T(0, y, t) = \theta_0(t) \qquad \mathbf{x} \in \Gamma_D \quad (2a)$$

$$\bar{n} \cdot \nabla T(\mathbf{x}, t) = \alpha(T_\infty(t) - T(\mathbf{x}, t)) + \varepsilon\sigma_{\mathrm{SB}}\big(T_\infty(t)^4 - T(\mathbf{x}, t)^4\big) \qquad \mathbf{x} \in \Gamma'_N \quad (2b)$$

$$\bar{n} \cdot \nabla T(\mathbf{x}, t) = 0 \qquad \mathbf{x} \in \Gamma''_N. \quad (2c)$$

In (2), α is the convective heat transfer coefficient, ε the emissivity of the strip, σ_{SB} the Stefan-Boltzmann constant, $T_\infty(t)$ the ambient temperature, and $\bar{n}$ the outward unit normal vector. The consistent initial condition is defined as $T(\mathbf{x}, 0) = T_0(\mathbf{x})$ for $\mathbf{x} \in \Omega_s$.

2.2 Heat Flux due to Inductive Heating

The computation of the volumetric heat source $\dot{q}_{\mathrm{IH}}(\mathbf{x}, I)$ requires the solution of Maxwell's equations. In the following, the 2D electromagnetic field problem from Fig. 2 is formulated.

A challenging part when modeling IH of ferromagnetic materials is the incorporation of the generally nonlinear material behavior in the Maxwell equations. This is due to nonlinearity, anisotropy, hysteresis, and saturation effects that characterize the electromagnetic behavior of steel strips. In the most general case, the flux density $\mathcal{B}(\mathbf{x}, t)$ and the magnetic field $\mathcal{H}(\mathbf{x}, t)$ are coupled by a nonlinear vector relation of the form (Meunier, 2008)

$$\mathcal{H}(\mathcal{B}) = \begin{cases} \frac{1}{\mu_0}\mathcal{B} - \mathcal{M}(\mathcal{B}), & \mathbf{x} \in \Omega_s \\ \frac{1}{\mu_0}\mathcal{B}, & \text{else.} \end{cases} \quad (3)$$

$\mathcal{M}(\mathcal{B})$ is the magnetization as a function of $\mathcal{B}(\mathbf{x}, t)$ and μ_0 denotes the permeability of vacuum. Various sophisticated models, e.g., the Preisach and the Jiles-Atherton model, can be found in the literature to describe $\mathcal{M}(\mathcal{B})$. The selection of such a model always involves a trade-off between accuracy and computational costs. Subsequently, in view of elevated strip temperatures, while still below the Curie point, a soft-magnetic material with a narrow hysteresis loop is assumed. As a consequence, only a marginal amount of heat is produced due to hysteresis losses such that a nonlinear anhysteretic relation formulated in terms of the norm amplitudes H and B is justified.

It is well known that for a time-harmonic excitation of the coils in the frequency range $f < 10\,\mathrm{MHz}$ the displacement current density is negligible compared to the conduction current density (Rudnev et al., 2017). With this approximation and (3), Maxwell's equations for the LFIH simplify to

$$\sigma\partial_t\mathcal{A}(\mathbf{x}, t) + \nabla \times \big(\mu_0^{-1}\nabla \times \mathcal{A}(\mathbf{x}, t)\big) = \mathcal{F}(\mathcal{B}, I) \quad (4a)$$

where

$$\mathcal{F}(\mathcal{B}, I) = \begin{cases} \mathcal{J}_{\mathrm{imp}}(I), & \mathbf{x} \in \Omega_c \\ \nabla \times \mathcal{M}(\mathcal{B}), & \mathbf{x} \in \Omega_s \\ 0, & \mathbf{x} \in \Omega_a. \end{cases} \quad (4b)$$

$\mathcal{A}(\mathbf{x}, t)$ is the magnetic vector potential which defines $\mathcal{B}(\mathbf{x}, t) = \nabla \times \mathcal{A}(\mathbf{x}, t)$. The electrical conductivity is denoted by σ. $\mathcal{A}(\mathbf{x}, t)$ evolves in the direction of the impressed current density $\mathcal{J}_{\mathrm{imp}}(I) = [0\ 0\ \sqrt{2}I(t)\sin(\omega t)/A_c]^{\mathrm{T}}$ with the cross-sectional surface A_c of a single coil.

For numerical simulations, (4) has to be complemented with boundary conditions. Their selection is a crucial point because the electromagnetic field extends in fact into an infinite spatial domain. In this work, the spatial domain Ω is extended by an exterior region (not shown in Fig. 2) where so called infinite elements are employed, (cf., Jin, 2014).

Formally, the heat source due to IH is defined by the Joule heat $\dot{q}_{\mathrm{IH}}(\mathbf{x}, I) = \mathcal{J}^{\mathrm{T}}\mathcal{E}$ with the current density $\mathcal{J}(\mathbf{x}, t)$ and the electric field $\mathcal{E}(\mathbf{x}, t)$. From Ohm's law $\mathcal{J}(\mathbf{x}, t) = \sigma\mathcal{E}(\mathbf{x}, t)$ for $\mathbf{x} \in \Omega_s$ together with Faraday's law of induction $\mathcal{E}(\mathbf{x}, t) = -\partial_t\mathcal{A}(\mathbf{x}, t)$, it follows that

$$\dot{q}_{\mathrm{IH}}(\mathbf{x}, I) = \sigma\left|\partial_t A_z(\mathbf{x}, t)\right|^2. \quad (5)$$

In (5), $A_z(\mathbf{x}, t)$ denotes the out-of-plane component of $\mathcal{A}(\mathbf{x}, t)$. For the considered LFIH, the frequency of the AC current is close to 100 kHz. Hence, the dynamics of the electromagnetic system is significantly faster than the dynamics of the thermal model (1)–(2). To avoid an excessive computational load when solving this two-time-scale problem, only the effective eddy current values following from the steady-state (harmonic) solution of (4) are used in (1). However, the computation of the steady-state solution of (4) is complicated by the fact that (3) defines a nonlinear relation. In the following subsection, an approach is introduced that facilitates the consideration of a nonlinear relation $H(B)$.

2.3 Effective Magnetization Approach

As reported by Paoli et al. (1998), the main idea of the so-called effective magnetization approach is the introduction of a fictitious material that approximates the nonlinear behavior of the ferromagnetic material. This fictitious material is described by a linear effective B_{eff}-H_{eff} curve with sinusoidal field quantities. There are several possibilities to construct this effective curve from a given nonlinear relation $H(B)$. In this paper, the energy method of Paoli et al. (1998) is used. It determines the relation $H_{\mathrm{eff}}(B_{\mathrm{eff}})$ in such a way that the magnetic energy $w_{\mathrm{eff}} = H_{\mathrm{eff}}B_{\mathrm{eff}}/2$ stored in the linear fictitious material is equal to the magnetic energy $w(B)$ stored in the strip.

The construction of the B_{eff}-H_{eff} curve is outlined in Fig. 3. For a given flux density $B_{\mathrm{eff}} = B$, the calculation of H_{eff} follows from the requirement that $w(B) = H_{\mathrm{eff}}B_{\mathrm{eff}}/2$. This yields the relation

$$H_{\mathrm{eff}}(B) = \frac{2}{B}\int_0^B H(B)\mathrm{d}B. \quad (6)$$

In practice, the B-H curve is often obtained from experimental measurements. Different methods for monotonicity-preserving analytical approximations of experimental B-H data are summarized by Pechstein and Jüttler (2006). In the current paper, a modified ansatz of Brauer (1975) is used to parameterize the original B-H curve by

$$H(B) = \xi_1 B + \xi_2(\exp(\xi_3 B) - 1), \quad \boldsymbol{\xi} = [\xi_i]_{i=1,\ldots,3} \quad (7)$$

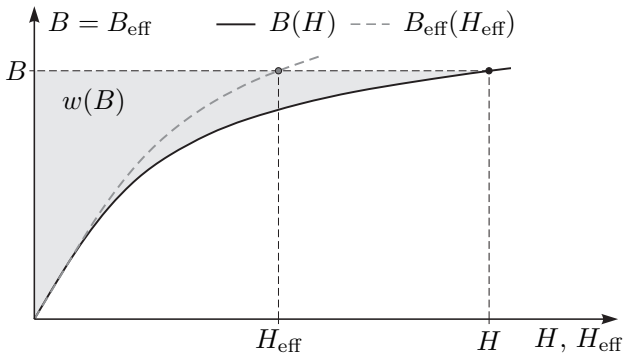

Fig. 3. An effective magnetization approach based on the energy method.

with constant parameters $\xi_i > 0$, $i = 1, 2, 3$. The ansatz ensures the monotonicity and $H(0) = 0$. Substitution of (7) into (6) yields the effective curve as

$$H_{\text{eff}}(B) = \eta_1 B + \eta_2 \frac{\exp(\eta_3 B) - 1}{B} - \eta_2 \eta_3 \tag{8}$$

with $\boldsymbol{\eta}(\boldsymbol{\xi}) = [\eta_i]_{i=1,\dots,3}$ and the bijective mapping $\eta_1 = \xi_1$, $\eta_2 = 2\xi_2/\xi_3$ and $\eta_3 = \xi_3$. For a linear original material, i.e., $\xi_2 = 0$, it follows $H_{\text{eff}}(B) = H(B) = \xi_1 B$. The inverse mapping $\boldsymbol{\xi}(\boldsymbol{\eta})$ is used in Section 4 to estimate the original H-B curve.

The effective magnetization approach together with the Coulomb gauge $\nabla \cdot \mathcal{A}(\mathbf{x}, t) = 0$ allows to rewrite (4) in the time-harmonic form

$$j\omega\sigma \hat{A}_z(\mathbf{x}) + \mu_{\text{eff}}^{-1} \Delta \hat{A}_z(\mathbf{x}) = \begin{cases} \hat{J}_{\text{imp},z}(I), & \mathbf{x} \in \Omega_c \\ 0, & \text{else,} \end{cases} \tag{9}$$

with the effective permeability

$$\mu_{\text{eff}} = \begin{cases} \frac{B}{H_{\text{eff}}(B)}, & \mathbf{x} \in \Omega_s \\ \mu_0, & \text{else.} \end{cases} \tag{10}$$

$\hat{A}_z(\mathbf{x})$ and $\hat{J}_{\text{imp},z}(I)$ are z-components of the complex-valued phasors of $\mathcal{A}(\mathbf{x}, t)$ and $\mathcal{J}_{\text{imp}}(I)$ from (4), respectively. Moreover, by time averaging of $\dot{q}_{\text{IH}}(\mathbf{x}, I)$ over one period $\Delta t = 2\pi\omega^{-1}$, it follows from (5) that

$$\dot{q}_{\text{IH}}(\mathbf{x}, I) = \frac{1}{2}\sigma\omega^2 \hat{A}_z(\mathbf{x}) \hat{A}_z(\mathbf{x})^* \tag{11}$$

with the complex conjugate $\hat{A}_z(\mathbf{x})^*$ of $\hat{A}_z(\mathbf{x})$.

The electromagnetic subsystem (9)–(11) and the thermal subsystem (1)–(2) constitute the mathematical model of the LFIH. Its numerical solution is computed by the FEM software COMSOL MULTIPHYSICS. The backward differentiation formula of order 2 with a constant sampling time t_s is used for numeric integration along the time domain.

3. MODEL VALIDATION

Where possible, the 2D LFIH model is parametrized with nominal dimensions and material parameters. However, to improve the model accuracy, selected parameters are additionally identified based on measurements recorded at the considered industrial plant under normal production conditions. The results of the model validation based on this parameter identification are subsequently presented.

Let $T_L(t) = 2\int_0^{\frac{B_s}{2}} T(L_s, y, t)\mathrm{d}y/B_s$ denotes the simulated mean strip temperature at the exit of the LFIH. By processing a steel strip with known B-H curve, the electric conductivity σ, the heat transfer coefficient α, and the strip emissivity ε are identified. With measurements and input signals recorded during the period $[0, \tau]$, the minimization problem

$$\min_{\mathbf{p}} \frac{1}{\tau}\int_0^\tau \left(\theta_L(t) - T_L(t)\right)^2 \mathrm{d}t, \tag{12}$$
$$\text{s.t. (1)–(2) \& (9)–(11)}$$

with $\mathbf{p} = [\sigma, \alpha, \varepsilon]$ is solved using the MATLAB routine `fmincon`. The required underlying evaluation of the mathematical model of the LFIH is carried out in COMSOL using the interface LIVELINK FOR MATLAB. The optimum cost function value found in (12) is less than 0.39 % of the time-averaged measured temperature T_{ref} in the time period $t = [0\ \tau]$.

The optimum values from (12) are $\sigma = 0.71 \times 10^6\,\text{S/m}$, $\alpha = 398\,\text{W/m}^2\text{K}$, and $\varepsilon = 0.78$. These values are henceforth used in the LFIH model. It has been validated by comparison with measurement results, which are shown in Fig. 4. Figure 4 (top) shows the measured and computed normalized mean strip temperature at the LFIH exit. The model accurately captures both the dynamics and the steady-state values of the strip temperature. The corresponding normalized input variables $\theta_0(t)$ and $I(t)$ are given in the middle and bottom picture of Fig. 4, respectively. The validated model is subsequently used to estimate unknown B-H curves of the strip at elevated temperatures.

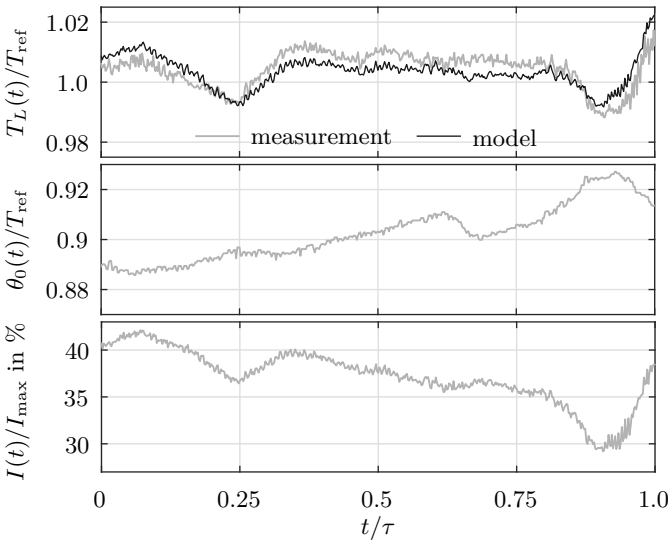

Fig. 4. Validation results: calculated $T_L(t)$ and measured $\theta_L(t)$ strip temperature at the furnace exit (top), measured strip temperature $\theta_0(t)$ at the furnace entrance (middle), normalized RMS current $I(t)$ (bottom).

4. IN-LINE ESTIMATION OF THE B-H CURVE

In the following, an MHE scheme for on-line identification of the unknown B-H curve of the strip material is developed. By utilizing the validated LFIH model, the unknown parameter vector $\boldsymbol{\xi}$, see (7), is estimated by minimizing the squared deviation between the calculated strip temperatures $T_L^i = T_L(it_s)$ and the corresponding measurement values $\theta_L^i = \theta_L(it_s)$. In each estimation horizon, $N + 1$

measured data points are used. The time span between two subsequent horizons is nt_s, with $n < N$.

The proposed MHE scheme is thus based on the solution of the minimization problem

$$\min_{\boldsymbol{\eta}_k} \sum_{i=nk-N}^{nk} \left(\theta_L^i - T_L^i\right)^2, \quad n, N \in \mathbb{N}_+ \tag{13}$$
$$\text{s.t. (1)–(2) \& (9)–(11)}$$

for a time-step $k \in \mathbb{N}_0$. Because of the computational load entailed by the LFIH model, an exact solution of (13) would prevent the real-time application of this MHE scheme. Therefore, a suboptimal solution $\boldsymbol{\eta}_k$ of (13), found by a single iteration of the MATLAB routine `fmincon`, is accepted. For this, the interior-point line-search algorithm with the numerical approximation of the gradient of the cost function in (13) is employed. The obtained values $\boldsymbol{\eta}_k$ are used as initial guess in the subsequent horizon. Finally, the parameters that control the B-H curve (7) are found in the form

$$\hat{\boldsymbol{\xi}}_k = \boldsymbol{\xi}(\boldsymbol{\eta}_k) = \begin{bmatrix} \eta_{1,k} \\ \frac{1}{2}\eta_{2,k}\eta_{3,k} \\ \eta_{3,k} \end{bmatrix}. \tag{14}$$

Both the horizon length N and the shifting distance n are tuning parameters of (13). It is well known that the convergence properties of MHE improves if the length N is increased. Clearly, this also entails higher computational costs. Therefore, a reasonable trade-off is required between the convergence rate of the MHE and the computational time. For the convergence analysis of a real-time MHE scheme, the reader is referred to (Wynn et al., 2014).

Remark 1. The MHE optimization problem (13) uses an arrival cost of zero, which means that information from measurements prior to the beginning of the current horizon is neglected. In general, the determination of the (full information) arrival costs is a challenging task, especially when dealing with constrained nonlinear systems. Different possibilities are reported in the literature in this context. To approximate the arrival cost, Rao and Rawlings (2002) used the extended Kalman filter, Qu and Hahn (2009) proposed the unscented Kalman filter, and López-Negrete et al. (2011) considered particle filters.

5. ESTIMATION RESULTS

In the following simulation experiment, a steel strip with a known B-H curve is considered. The B-H curve is known from laboratory measurements, which allows the calculation of the nominal parameters ξ_i, $i = 1, \ldots, 3$ used in (7) by solving a nonlinear least squares problem. The goal is to recalculate this B-H curve by means of the MHE as proposed in Section 4. Hence, the MHE scheme is initialized at the time $t = 0$ with the intentionally incorrect values $\hat{\xi}_i = 0.6\xi_i$, $i = 1, \ldots, 3$. For the estimation, real measurements of the process variables during the time period $t = [0\ t_E]$ are used. To evaluate the performance of the proposed MHE approach, its estimation results are compared with the nominal parameters. In (13), the horizon size is set to $N = 20$ and the shifting distance is chosen as $n = 10$.

The obtained estimation results are presented in Fig. 5. The top half of Fig. 5 contains the evolution of the normalized parameters $\hat{\xi}_i$, $i = 1, \ldots, 3$. They are constant and equal to their (incorrect) initial values for $t < 0.2t_E$. During this period, the MHE is switched off. At the time $t = 0.2t_E$, the MHE is switched on and the parameter estimates $\hat{\xi}_i$ evolve towards their nominal values ξ_i. After a transient period of just 6 estimation horizons, the estimates $\hat{\xi}_2$ and $\hat{\xi}_3$ deviate less than 5.2 % and 2.9 %, respectively, from their nominal values. The parameter ξ_1 is estimated with a slightly higher inaccuracy and slightly more fluctuations, which has the following reasons. First, the IH process typically causes saturation on the strip material. In this case, the nonlinear term in (7) dominates and the sensitivity of the strip temperature θ_i with respect to ξ_1 is low. Second, the chosen ersatz of the B-H curve may fail to exactly reproduce the true B-H curve, which inevitably entails an uncertain model-plant mismatch. However, Fig. 5(d) demonstrates that the proposed MHE achieves an excellent estimation accuracy in terms of the B-H curve compared to laboratory measurements. This is ensured despite the significant deviation of the initial B-H curve from the experimental data and a very limited magnetic field excitation in the strip in the range between 2.4×10^3 A/m and 3×10^3 A/m. The limited field excitation indicated by the gray area in Fig. 5(d) corresponds to the time evolution of the strip-averaged magnetic field H_{mean} shown in Fig. 5(e).

A comparison of the simulated exit temperature error $e_i = \theta_L^i - T_L^i$ is presented in Fig. 5(f). The observed initial temperature deviation of about 3 % quickly decreases after the MHE is activated. For $t > 0.3t_E$, the relative temperature error $|\theta_L^i - T_L^i|/T_{\text{ref}}$ never exceeds 0.5 %.

6. CONCLUSIONS

In this paper, an in-line estimation strategy for the magnetic properties of a steel strip in an inductive heating (IH) system was developed and investigated. The proposed moving horizon estimator (MHE) approach achieves an accurate identification of the B-H curve at elevated temperatures. The MHE is based on an optimization problem with an objective function that sums up the error of the mean strip exit temperature. As a basis for the optimization problem, the 2D finite element (FE) temperature model of the strip was developed and implemented in the FE software COMSOL. The heat source due to the IH system is calculated from the nonlinear Maxwell equations. The effective magnetization approach allows an approximation of the nonlinear Maxwell equations by a linear time-harmonic formulation. In fact, a fictitious linear material is used to approximate the nonlinear B-H curve of the original strip material. This curve is mathematically described by a linear and an exponential function, which allows a direct calculation of the parameters of the fictitious material. The proposed MHE scheme achieves an excellent estimation performance and a high convergence speed, even if a suboptimal solution of the underlying optimization problem is accepted. The in-line estimated B-H curve accurately agrees with laboratory measurements.

REFERENCES

Baker, R.M. (1945). Induction heating of moving magnetic strip. *Electrical Engineering*, 64(4), 184–189.

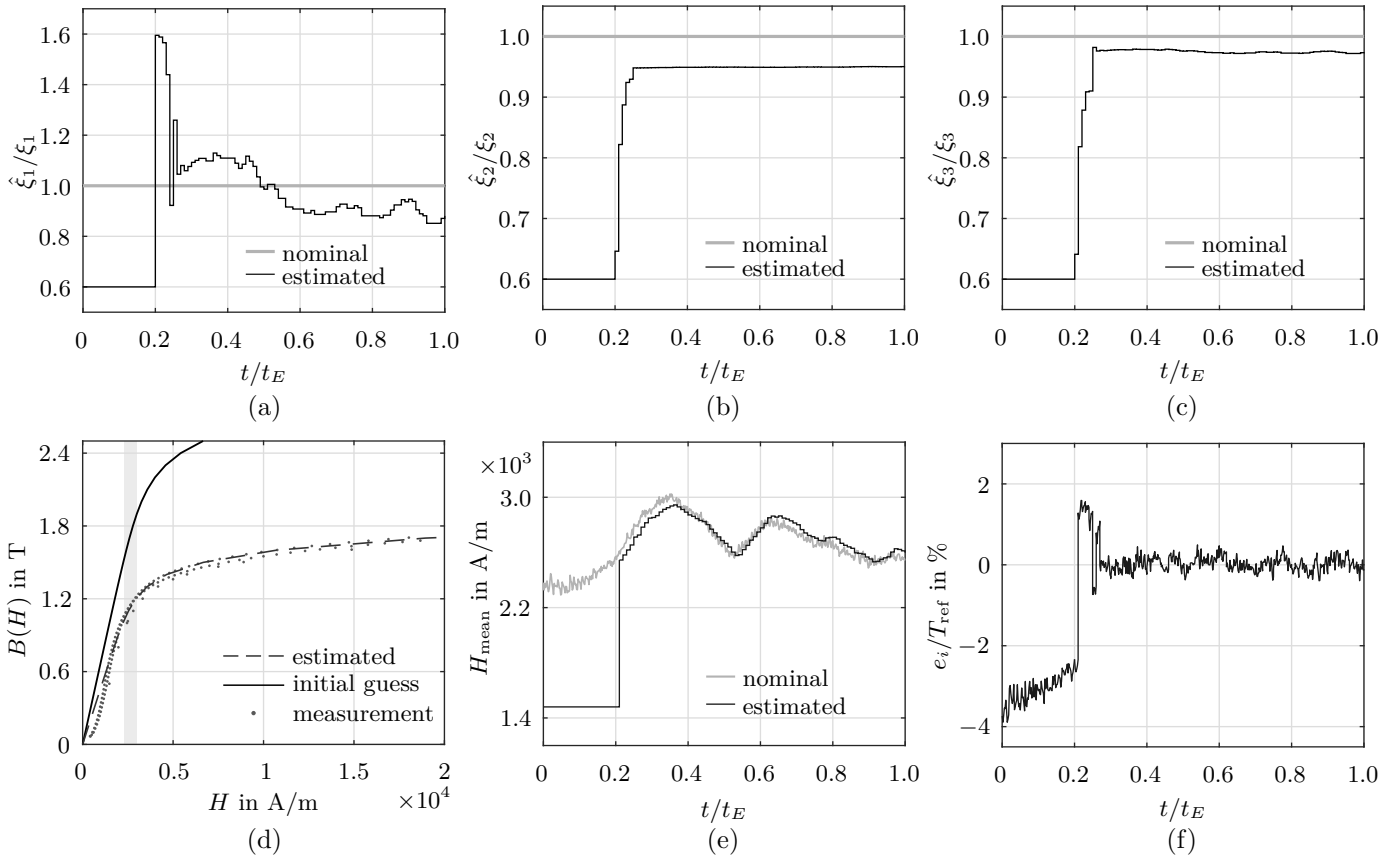

Fig. 5. Estimation performance of the MHE scheme: (a) parameter $\xi_{1,k}$, (b) parameter $\xi_{2,k}$, (c) parameter $\xi_{3,k}$, (d) known and estimated $B(H)$ curve. Gray area indicates the limited excitation range resulting from the applied heating power. (e) Strip-averaged magnetic field strength, (f) normalized temperature error.

Bozorth, R. (2003). *Ferromagnetism*. John Wiley & Sons, Hoboken.

Brauer, J. (1975). Simple equations for the magnetization and reluctivity curves of steel. *IEEE Transactions on Magnetics*, 11(1), 81–81.

Hao, X., Yin, W., Strangwood, M., Peyton, A., Morris, P., and Davis, C. (2010). Modelling the electromagnetic response of two-phase steel microstructures. *NDT & E International*, 43(4), 305 – 315.

Jin, J.M. (2014). *The Finite Element Method in Electromagnetics*. John Wiley & Sons, Hoboken, 3rd edition.

López-Negrete, R., Patwardhan, S.C., and Biegler, L.T. (2011). Constrained particle filter approach to approximate the arrival cost in moving horizon estimation. *Journal of Process Control*, 21(6), 909 – 919.

Meunier, G. (2008). *The Finite Element Method for Electromagnetic Modeling*. John Wiley & Sons, Hoboken.

Paoli, G., Biro, O., and Buchgraber, G. (1998). Complex representation in nonlinear time harmonic eddy current problems. *IEEE Transactions on Magnetics*, 34(5), 2625–2628.

Pechstein, C. and Jüttler, B. (2006). Monotonicity-preserving interproximation of B–H-curves. *Journal of Computational and Applied Mathematics*, 196(1), 45 – 57.

Qu, C.C. and Hahn, J. (2009). Computation of arrival cost for moving horizon estimation via unscented kalman filtering. *Journal of Process Control*, 19(2), 358 – 363.

Rao, C.V. and Rawlings, J.B. (2002). Constrained process monitoring: Moving-horizon approach. *AIChE Journal*, 48(1), 97–109.

Roetzer, F., Aschauer, A., Jadachowski, L., Steinboeck, A., and Kugi, A. (2020). Temperature Control for Induction Heating of Thin Strips. Accepted to the 21st IFAC World Congress – Berlin, Germany, 12–17 Jul. 2020.

Rudnev, V., Loveless, D., and Cook, R. (2017). *Handbook of Induction Heating*. Manufacturing Engineering and Materials Processing. CRC Press, Boca Raton, 3rd edition.

Saxinger, M., Marko, L., Steinboeck, A., and Kugi, A. (2018). Active rejection control for unknown harmonic disturbances of the transverse deflection of steel strips with control input, system output, sensor output, and disturbance input at different positions. *Mechatronics*, 56, 73 – 86.

Shen, J., Zhou, L., Jacobs, W., Hunt, P., and Davis, C. (2019). Real-time in-line steel microstructure control through magnetic properties using an EM sensor. *Journal of Magnetism and Magnetic Materials*, 490, 165504.

Skarlatos, A., Reboud, C., Svaton, T., Martinez-de Guerenu, A., Kebe, T., and van den Berg, F. (2016). Modelling the impoc response for different steel strips. In *19th World Conference on Non-Destructive Testing (WCNDT 2016)*. Munich, Germany. 13–17 Jun. 2016.

Wynn, A., Vukov, M., and Diehl, M. (2014). Convergence guarantees for moving horizon estimation based on the real-time iteration scheme. *IEEE Transactions on Automatic Control*, 59(8), 2215–2221.